LASER & PHOTONICS REVIEWS

www.lpr-journal.org

Compact High Resolution Speckle Spectrometer by Using Linear Coherent Integrated Network on Silicon Nitride Platform at 776 nm

*Zunyue Zhang, Yuan Li, Yi Wang, Zejie Yu, Xiankai Sun, and Hon Ki Tsang**

Motivated by applications in mobile optical sensing, ultracompact high-resolution integrated spectrometers have attracted much interest. Here, a high-resolution integrated speckle spectrometer, comprising a linear coherent network formed by mutually coupled Mach–Zehnder interferometers and nonidentical microring resonators, is proposed and demonstrated. Deep-etched grating lines used as mirrors on the edges of the coherent network increase the effective optical path lengths. The speckle spectrometer is realized on a silicon nitride platform, operating at 776 nm central wavelength. The eight-in—eight-out linear coherent network provides 64 physical channels. Fine spectral lines separated by 20 pm are experimentally resolved within a device footprint of 520 μm × 220 μm. Compressive sensing is achieved for sparse spectra over a wide optical bandwidth. Up to 600 distinctive wavelength channels can be reconstructed from the 64 physical channels, giving 12 nm operating bandwidth. Both sparse spectra and continuous spectra are well reconstructed experimentally. The integrated speckle spectrometer has great potential for use in future biosensing and bioimaging applications where high spectral resolution is desired.

1. Introduction

Integrated optical spectrometers have applications in numerous fields, such as chemical engineering,[1] astronomical spectroscopy,[2] biosensing, and bioimaging.[3,4] Previous approaches to implement conventional integrated optical spectrometers rely on spectral to spatial mapping, including the use of echelle gratings,[5] arrayed waveguide gratings,[6,7] digital planar holography,[8] and photonics crystals.[9] However, attaining high spectral resolution in a compact footprint remains very challenging because the spectral resolution in conventional spectrometers is inversely proportional to the size of the spectrometer.

Z. Zhang, Y. Li, Y. Wang, X. Sun, H. K. Tsang
Department of Electronic Engineering
The Chinese University of Hong Kong
Shatin, New Territories, Hong Kong SAR, P. R. China
E-mail: hktsang@ee.cuhk.edu.hk
Z. Yu
College of Optical Science and Engineering
Zhejiang University
Hangzhou, Zhejiang 310058, P. R. China

The ORCID identification number(s) for the author(s) of this article can be found under https://doi.org/10.1002/lpor.202100039

DOI: 10.1002/lpor.202100039

Optical spectrometers which rely on the alternative approach of utilizing wavelength-dependent speckle patterns have attracted increasing research interest.[10–24] The speckle patterns created by the light scattering in the integrating sphere[12,13] and Rayleigh backscattering in the single mode fiber[14,15] have been demonstrated to offer sub-femtometer spectral resolution with wide optical bandwidth. The intermodal interference in the multimode fiber provides another lossless approach of speckle spectrometer.[16–20] However, the weak dispersion of optical fibers makes it necessary to use long fiber to attain high spectral resolution. Integrated photonics offers the opportunity to realize the miniaturized speckle spectrometers on chip. The speckle spectrometers based on disordered photonic chip have been demonstrated to offer high spectral resolution and ultracompact footprint.[21,22] However, the unavoidable scattering loss introduces a significant trade-off in loss (spectrometer sensitivity) for improved spectral resolution by increasing the size of the scattering medium. The speckle spectrometers by using multimode waveguide offer the potential for higher spectral resolution with lower loss.[23,24] However, the increasing bending loss of the multimode waveguides hinders the usage of sharper bends and further miniaturization of the spectrometer for large-scale integration.

In this paper, a compact high-resolution speckle spectrometer was proposed by using an integrated linear coherent network formed by - mutually coupled Mach–Zehnder interferometers (MZI) and microring resonators (MRRs), as illustrated in **Figure 1**a. On-chip mirrors formed by deep-etched grating lines are used on the edges of the linear coherent network to enable both forward and backward propagation of light and further increase the optical path length. Instead of using the intermodal interference in the multimode waveguides, the wavelength-dependent speckle patterns are created by the interference in the linear coherent network formed by single-mode waveguides, where much sharper bends can be used with low bending loss, the compact footprint of the speckle spectrometer can thus be reduced.

The MZI-based linear coherent networks integrated in a silicon photonic circuit have been widely studied and used as optical interference units to implement linear matrix-vector

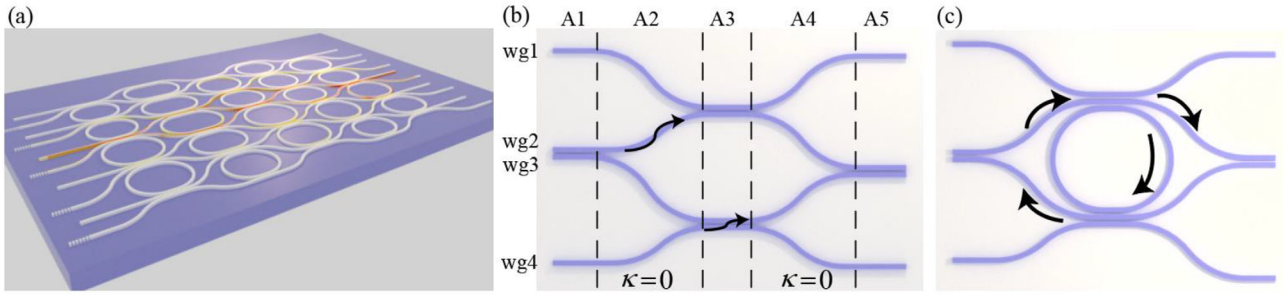

Figure 1. a) Schematic of the speckle spectrometer. b) Schematic of one building block of the mutually coupled MZIs, where κ is the coupling coefficient. c) Schematic of one building block of the linear coherent network with MRR added into the mutually coupled MZI.

multiplication in the optical neural networks,[25–27] which shows its potential in large-scale integration with low propagation loss. To enhance the diversity of optical path lengths in the network required by a high-resolution speckle spectrometer, MRRs are introduced to provide efficient wavelength-dependent phase shift around the resonance wavelengths[28] and compensate the insufficient dispersion provided by MZI network. Moreover, the round-trip path of the MRR also enables backward propagation of the light in the speckle spectrometer, which increases the physical path length and further improves the spectral resolution.

The proof-of-concept demonstration was implemented on a silicon nitride platform. Silicon nitride has a smaller thermo-optic coefficient than silicon and has the advantage of being less temperature sensitive. A cross measurement procedure was conducted with light launched from one of the input ports at a time and measured from all the output ports. Eight inputs and eight outputs can thus give 64 physical channels. Unlike conventional one-to-one spectral-to-spatial mapping, in the speckle spectrometer, each wavelength is projected to all the spatial channels. Compressive sensing (CS) methodology is used to reconstruct the sparse spectra over a wide operating bandwidth. With the constraint of having a sparse spectrum of only two lines, the optical bandwidth of the spectrometer can far exceed the number of the physical channels. Operation of the spectrometer with up to 12 nm optical bandwidth and 20 pm spectral resolution was experimentally demonstrated within a device footprint of 520 μm × 220 μm.

2. Spectrometer Design

As illustrated in Figure 1a, when the light of a certain wavelength is coupled into the speckle spectrometer through one of the input ports, it will spread in the linear coherent network and arrive at the output ports with a distinctive intensity distribution. The output light intensity from each channel is formed by the interference of light reaching the same output channel from completely different optical paths. Due to the dispersion in the linear coherent network and the excess phase delay introduced by MRRs, different wavelengths will have different optical paths and thus produce different intensity and phase distributions, which finally lead to a variation in the interference speckle pattern with wavelength. By placing mirrors on the edges of the linear coherent network, the optical path lengths can be effectively increased and a more diverse phase distribution can be obtained, giving rise to a more rapid decorrelation of the speckle pattern with wavelength.

The two basic building components in the coherent network are mutually coupled MZIs (Figure 1b) and MRRs (Figure 1c). Limited by the weak dispersion in the mutually coupled MZIs, the optical path length differences between wavelengths would be insufficient to create a rapid decorrelation in the speckle patterns, and longer optical paths are needed to enhance the optical path length diversity. Mirrors formed by deep-etched grating lines are used at both edges of the coherent network to enable backward propagation of the light, which increases the effective diversity of optical path lengths in the coherent network.

To further enhance the diversity in optical path lengths, MRRs are introduced. The four-port MRRs, as illustrated in Figure 1c, enable back propagation of the light in the coherent network from the drop ports, which helps to increase the optical path length. On the other hand, considerable effective phase delay can be introduced around the resonance wavelengths. We numerically calculated the propagation of light in the coherent network and obtained the transmission matrix (see the Supporting Information for the modeling of the linear coherent network). **Figure 2**a shows the transmission matrix of the speckle spectrometer without MRRs and with all the building blocks of the mutually coupled MZIs set as identical. To evaluate the wavelength decorrelation of the speckle patterns created by the spectrometer, spectral correlation function was used[20]

$$C(\Delta\lambda, N) = \frac{\langle I(\lambda, N)\, I(\lambda + \Delta\lambda, N)\rangle}{\langle I(\lambda, N)\rangle\langle I(\lambda + \Delta\lambda, N)\rangle} - 1 \tag{1}$$

where $I(\lambda, N)$ represents the output light intensity of the physical channel N for input wavelength λ, $\Delta\lambda$ is the spectral spacing of two wavelengths, and <···> denotes the average over wavelengths. The average spectral correlation function over all physical channels is shown in Figure 2d. The spectral correlation width $\delta\lambda$ (half width at half maximum of $C(\Delta\lambda)$) is 0.71 nm, which indicates 0.71 nm wavelength difference can decorrelate the speckle patterns by 0.5. The spectral correlation function can thus be used as an estimation of the spectral resolution.

We then added MRRs into the coherent network. The single-trip lengths of the MRRs are initially set as identical. The simulated transmission matrix is shown in Figure 2b and the calculated C function is shown in Figure 2e. $\delta\lambda$ is reduced to 0.3 nm. With all the MRRs designed as identical, the effective

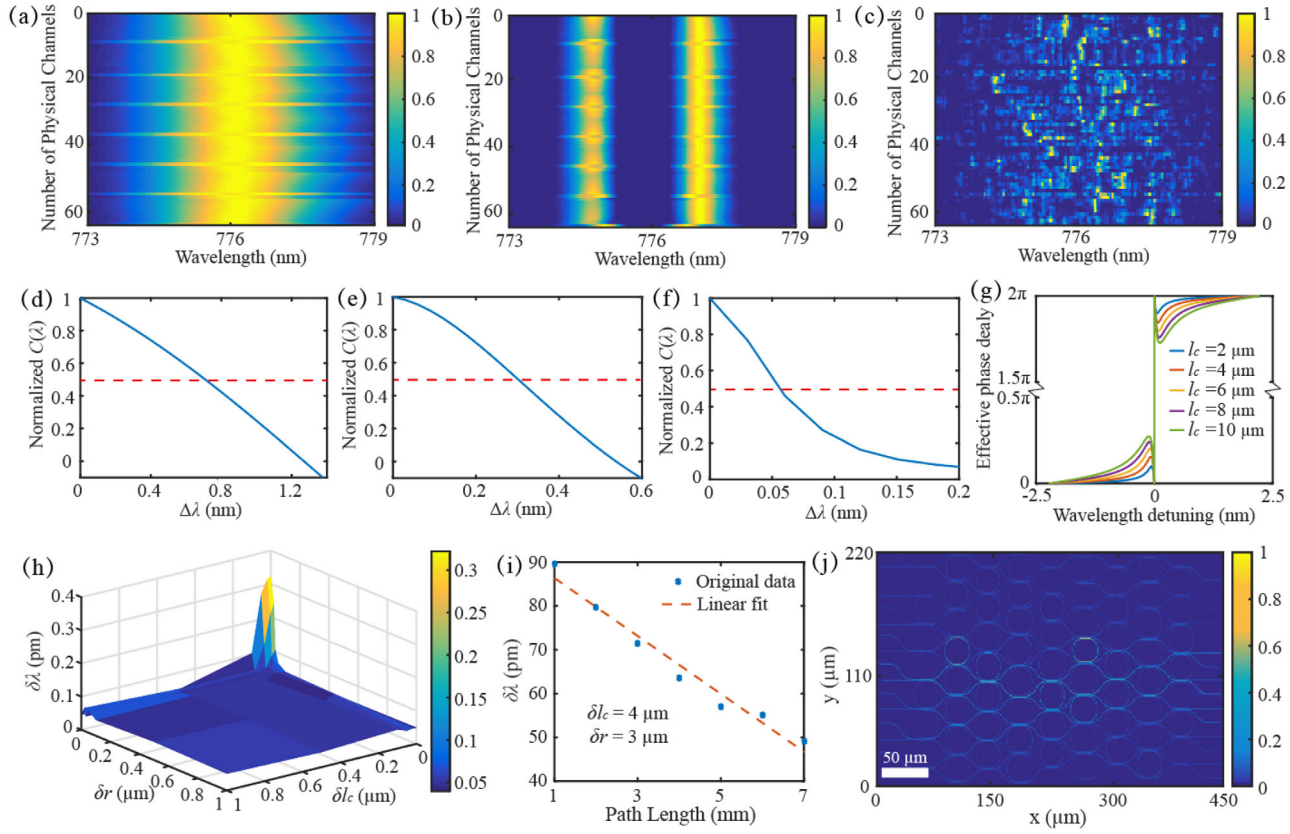

Figure 2. Simulated transmission matrix of the coherent network a) without MRRs, b) with MRRs but no random variations are added, c) with random variations in MRRs. Normalized spectral correlation function of the speckle spectrometers d) without MRRs, e) with MRRs but no random variations are added, f) with random variations in MRRs. g) Effective phase delay introduced by MRRs with different coupling length l_c of 2, 4, 6, 8, and 10 μm. h) Simulated spectral correlation width $\delta\lambda$ with different δl_c and δr. The total path length is 5 mm. i) Simulated spectral correlation width $\delta\lambda$ as a function of the total optical path length with $\delta l_c = 4$ μm and $\delta r = 3$ μm. j) Simulated optical field of light propagating in the designed speckle spectrometer by Lumerical 2.5D varFDTD solver.

phase delays introduced by different MRRs have the same distribution over wavelengths, and thus the variations of the speckle patterns with wavelengths are still limited. When the MRRs used in the coherent network are designed to be nonidentical, the diversity in the phase distribution over wavelengths can be greatly increased, and a rapid variation in the speckle patterns with wavelength can be obtained. The simulated transmission matrix of the speckle spectrometer after adding a random variation in MRRs is shown in Figure 2c and the corresponding C function is shown in Figure 2f. $\delta\lambda$ becomes 54 pm, which is a great improvement than the one with identical MRRs.

The MRRs are designed with a shape of racetrack, which separates the coupling length from the bend radius of the ring. Other than the single-trip path length, which determines the resonance wavelengths, the self-coupling coefficient in the directional coupler determines the effective phase delay when the round-trip loss in the MRR is fixed, as shown in Figure 2g. Random variations are added in both the coupling length (l_c) and bending radius (r) in the simulation. Figure 2h shows the simulated results of $\delta\lambda$ with different variations in both the coupling length δl_c and the bending radius δr. $\delta\lambda$ drops rapidly with the increase of δl_c and δr at the beginning. With the further increase of δl_c and δr, the decrease of $\delta\lambda$ becomes slower. As discussed above, the random variations in l_c and r of the MRRs introduce the extra phase differences between wavelengths. Therefore, when the random variations in l_c and r are large enough to provide 2π phase variations, the improvement on the spectral resolution will be significant, which indicates that the high spectral resolution in the proposed coherent network-based speckle spectrometer is easier to obtain by simply adding a small amount random variations in l_c and r compared with the multimode fiber-based speckle spectrometer where the improvement in spectral resolution needs to be obtained by increasing the fiber diameter.[29] δl_c and δr used in the speckle spectrometer are 4 and 3 μm, respectively. On the other hand, longer effective optical paths are desired to increase the differential phase change among closely spaced wavelengths and improve the spectral resolution. We simulated the output light intensity distribution of the speckle spectrometer with different total optical path lengths and calculated $\delta\lambda$ as a function of the total optical path length with $\delta l_c = 4$ μm and $\delta r = 3$ μm. The results are shown in Figure 2i. $\delta\lambda$ decreases approximately linearly with the increase of total optical path length, which indicates that longer optical path length provides higher spectral resolution. The dependence of the spectral resolution on the optical path length in the proposed speckle spectrometer is similar to the multimode fiber-based speckle spectrometer.[29] To keep

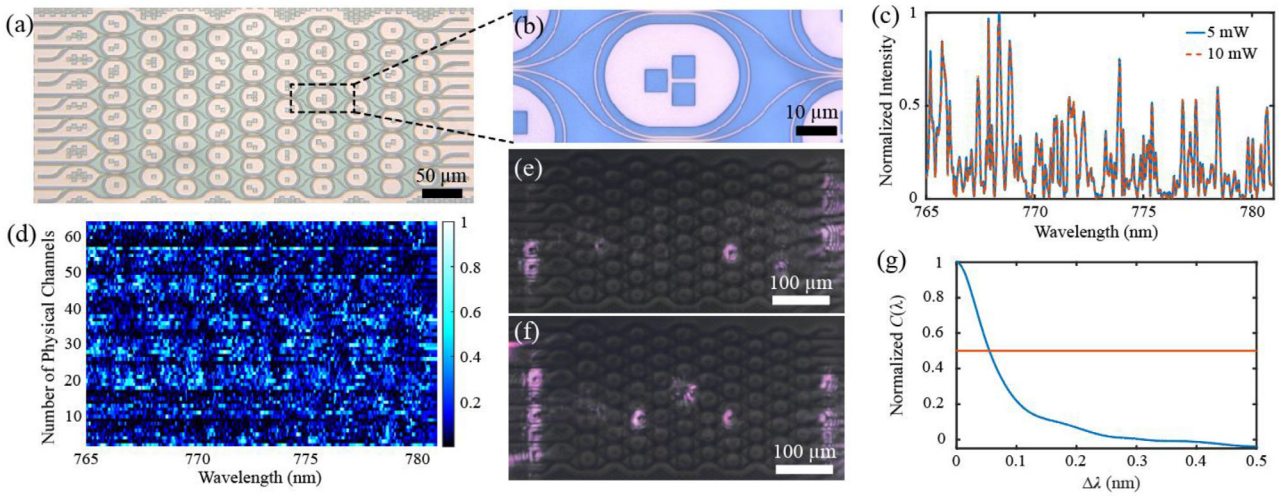

Figure 3. a) Optical microscope image of the integrated speckle spectrometer. b) Optical microscope image of one building block of the linear coherent network. c) Normalized transmission spectra of No. 32 physical channel with input light power of 5 and 10 mW. d) Calibration matrix of the speckle spectrometer. e,f) Scattering light from the on-chip spectrometer captured by infrared camera at 775.5 and 776 nm. g) Calculated spectral correlation function of the 64-channel speckle spectrometer.

the speckle spectrometer compact, the length of the coherent network is designed to be 500 μm. Assisted by the reflections from the on-chip mirrors, the effective path length is estimated to be 5 mm. The simulated optical field of light propagating in the designed speckle spectrometer by Lumerical 2.5D varFDTD solver is shown in Figure 2j.

3. Experimental Results

The device was fabricated by Interuniversity Microelectronics Centre (IMEC) on a silicon nitride multiproject wafer platform. The thickness of the silicon nitride layer is 300 nm, with 3 μm buried oxide and air cladding. The fabricated device is shown in **Figure 3**a. Figure 3b shows an enlarged view of one building block of the linear coherent network. The width of the waveguides used in the speckle spectrometer is 600 nm and the gap between waveguides in the directional couplers is 150 nm, which is designed as the minimum size allowed by the fabrication to provide the largest possible coupling dispersion.

To use the linear coherent network as a speckle spectrometer, the device was first calibrated with a tunable laser in the wavelength range of 765–781 nm with a wavelength scanning step of 1 pm. Light from the tunable laser was coupled onto the chip through fiber-waveguide grating couplers, and the output light from various output channels was also coupled through the grating couplers to a single-mode fiber and sent to optical power meter for measurement. The scattering light from the on-chip speckle spectrometer captured by an infrared camera indicates the different paths that different wavelengths follow. Figure 3e,f show the scattering fields from the chip at different wavelengths. The calibration matrix of the 64-channel speckle spectrometer is shown in Figure 3d. The C function is calculated as shown in Figure 3g. $\delta\lambda$ is calculated to be 55 pm, which is consistent with the theoretical estimation. The spectral resolution of speckle spectrometer can be improved by increasing the size of the linear coherent network to enable longer optical path lengths and include more MRRs. Due to the low loss of the single-mode silicon nitride waveguides, this improvement in spectral resolution will introduce negligible excess loss.

To verify the linearity of the speckle spectrometer, the calibration measurement was conducted with 5 mW and 10 mW input power, respectively. The normalized transmission spectra of No. 32 physical channel with different input power are shown in Figure 3c, which are consistent with each other and thus verify the linearity of the speckle spectrometer.

The spectral correlation function can only provide an estimation of the spectral resolution and the actual spectral resolution of the speckle spectrometer is determined by the minimum wavelength spacing that can be resolved by the spectrometer from the speckle patterns. The output intensity pattern was synthesized for an arbitrary input spectrum by adding up the output power from different physical channels measured at individual wavelengths. The transmission matrix T was extracted from the calibration matrix. As the output light intensity distribution I is related to the input spectrum S by $I = T{\cdot}S$, the unknown input spectrum can be calculated by multiplying the output light intensity I by the inverse matrix of T, i.e., $S = T^{-1}{\cdot}I$. To get rid of the experimental noise, nonlinear optimization was applied to find the input spectrum which can minimize $||I - T{\cdot}S||^2$. The Moore–Penrose pseudoinverse matrix[30] of T was used to calculate an initial spectrum S for the nonlinear optimization. Simulated annealing algorithm[31] was used in the spectrum recovery. To evaluate the accuracy of the reconstruction, the relative error was used

$$\varepsilon = \frac{\left[\sum_{i=1}^{M}\left(S - S_0\right)^2\right]^{1/2}}{\left[\sum_{i=1}^{M} {S_0}^2\right]^{1/2}} \tag{2}$$

where S is the recovered spectrum and S_0 is the original spectrum, M is the number of wavelength channels. When the two

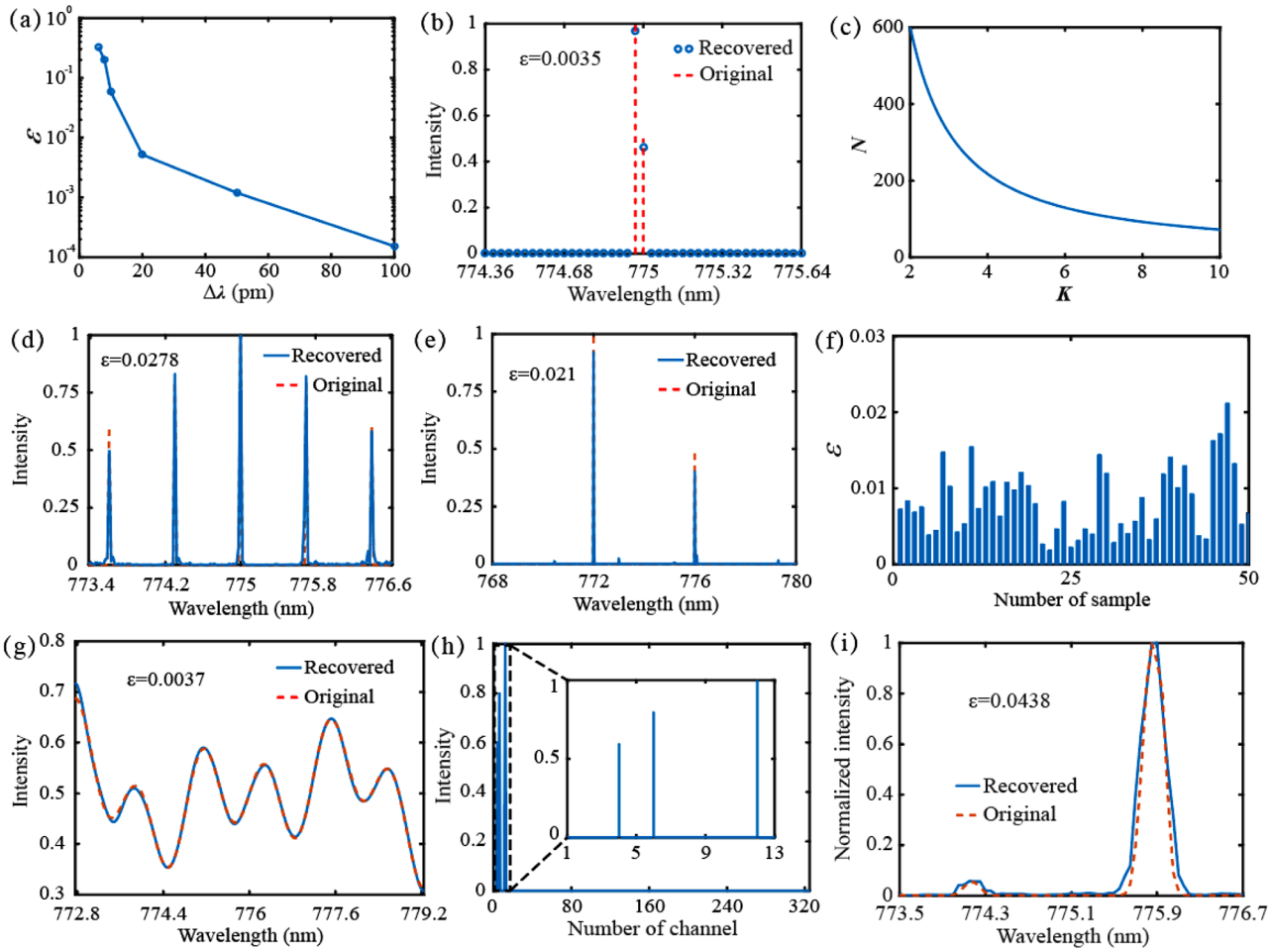

Figure 4. a) Relative errors of the recovered spectra with increasing wavelength spacing between the two spectral lines. b) Reconstructed spectral lines with spectral spacing of 20 pm. c) Number of the wavelength channels that can be recovered from the spectra with different sparsity. d) Reconstructed sparse spectra with 5 spectral lines in a 3.24 nm operating bandwidth. e) Reconstructed sparse spectra with two spectral lines in a 12 nm operating bandwidth. f) Relative errors of 50 reconstructed spectrum samples. g) Reconstructed continuous spectrum by nonlinear optimization in DCT domain. h) DCT of the spectrum in (g). i) Reconstructed result of the transmission spectrum of one channel of arrayed waveguide grating.

wavelengths get closer, the relative error in reconstruction increases, as shown in **Figure 4**a. Experimentally, two spectral lines separated by 20 pm can be well reconstructed by the speckle spectrometer with a relative error of 0.0035, as shown in Figure 4b.

Generally speaking, the number of wavelength channels that can be recovered is limited by the number of physical channels as the inverse matrix is only applicable to the square matrix, which leads to a trade-off between spectral resolution and optical operating bandwidth. However, when the input signals are sparse or compressible, compressed sensing (CS) can be applied to recover more wavelength channels from the limited physical channels than the conventional method.[32]

When the signal S has a sparse representation $S = \Psi\theta$, where Ψ is an $M \times M$ orthonormal basis matrix and only $K << M$ elements of θ are nonzero, the number of measurements required to reproduce S is given by $\text{const}\cdot K(\log M)^4$, where const is a constant that depends on each instant. The number of measurements of the speckle spectrometer is fixed to be 64. The number of wavelength channels that can be recovered, i.e., the bandwidth of the speckle spectrometer is thus determined by the sparsity of the input spectrum. Figure 4c shows the number of wavelength channels that can be recovered from the 64 physical channels when the sparsity of the input spectra changes. Figure 4d shows the recovered spectra of five spectral lines with specific intensity, which covers 162 wavelength channels with optical bandwidth of 3.24 nm. When the number of spectral lines is reduced to 2, a total of 600 wavelength channels can be recovered with optical bandwidth expanded to 12 nm. The recovered spectrum is shown in Figure 4e. The spectrum reconstruction process was repeated for 50 different samples and the relative errors of the reconstructions were calculated. The statistics result of the construction errors is shown in Figure 4f. To further enhance the operating bandwidth of the speckle spectrometer, the linear coherent network can be designed with more branches to enable more physical channels in the measurement and thus increase the number of wavelength channels that can be resolved.

Furthermore, the speckle spectrometer was also applied to recover the continuous spectrum. Although the spectrum is not sparse, a discrete cosine transform (DCT) can be conducted to

Table 1. Comparison of on-chip speckle spectrometers.

Spectrometer	Footprint	Resolution	Bandwidth	Platform
Disordered photonic chip[21]	50 μm × 25 μm	0.75 nm	25 nm	Silicon
Disordered photonic chip[22]	200 μm × 100 μm	4 nm	128 nm	Silicon nitride
Multimode spiral waveguide[24]	500 μm × 500 μm	0.01 nm	2 nm (4 spectral lines)	Silicon
Multimode waveguide and Photonic Lantern[23]	≈ 2.5 mm × 1.2 mm	0.1 nm	6.4 nm	Silicon
Coherent network (this work)	520 μm × 220 μm	0.02 nm	12 nm (2 spectral lines)	Silicon nitride

the continuous spectrum.[33] The continuous spectrum then becomes sparse in the DCT domain, where CS can still be applied to recover the spectral lines.[17] The nonlinear optimization was applied to minimize $||I - T^{DCT} \cdot S^{DCT}||^2$, with $T^{DCT} = T \cdot D^{-1}$ and $S^{DCT} = D \cdot S$, where D is the DCT matrix and is a real orthonormal matrix. Figure 4g shows the recovered continuous spectrum with three spectral lines in the DCT domain. The corresponding DCT spectrum is shown in Figure 4h. (see the Supporting Information for details of DCT of the continuous spectra).

As a concept demonstration, the speckle spectrometer was used to measure the transmission spectrum of an arrayed waveguide grating (AWG). Figure 4i shows the reconstructed spectrum of one AWG channel at center wavelength of 775.9 nm with a sidelobe at about 774.2 nm. The original spectrum is shown in dash line. The relative error of the reconstruction is 0.0438.

The performance of the proposed speckle spectrometer was compared with the other integrated speckle spectrometers implemented on either silicon on insulator platform or silicon nitride/silicon oxide/silicon platform in terms of footprint, spectral resolution, and optical bandwidth, as shown in **Table 1**. The proposed speckle spectrometer has a more compact footprint compared with the other speckle spectrometers that have comparable spectral resolutions. Benefitting from the compressive sensing technique, the spectral channel number (bandwidth/resolution) of the proposed speckle spectrometer can be much larger than the other speckle spectrometers when the input is limited to sparse spectra.

4. Conclusion

We proposed and demonstrated a compact high-resolution integrated spectrometer by using a linear coherent network. The wavelength-dependent speckle patterns, which are created in the mutually coupled MZIs assisted by nonidentical MRRs, can be used as the fingerprint of the individual wavelength. Enabled by the on-chip mirrors on the edges of the linear coherent network, both forward and backward light propagation can be obtained, and thus the optical paths are greatly elongated. The diversity of the optical path lengths accelerates the wavelength decorrelation and helps to increase the spectral resolution. The speckle spectrometer was experimentally demonstrated on a silicon nitride platform at 776 nm central wavelength with 520 μm × 220 μm spectrometer footprint. The cross measurement of the eight input ports and eight output ports gives 64 physical channels. Two spectral lines with spectral spacing of 20 pm can be experimentally resolved. When the input spectrum is sparse, compressive sensing can be applied to improve the optical operating bandwidth of the speckle spectrometer. Up to 600 wavelength channels can be experimentally reconstructed with 64 physical channels, giving an operating bandwidth of 12 nm. The recovery of both sparse spectra and continuous spectra are demonstrated. The integrated speckle spectrometer shows great potential for future biosensing and bioimaging applications where high spectral resolution is needed.

Supporting Information

Supporting Information is available from the Wiley Online Library or from the author.

Acknowledgements

The authors would like to thank IMEC for device fabrication in the BioPix program. This work was funded by Innovation and Technology Fund (ITF) projects ITS/433/17FX and MRP/066/20.

Conflict of Interest

The authors declare no conflict of interest.

Data Availability Statement

The data that support the findings of this study are available in the Supporting Information of this article.

Keywords

high-resolution spectrometer, linear coherent network, speckle spectrometer

Received: January 26, 2021
Revised: April 30, 2021
Published online: August 21, 2021

[1] S. Mallakpour, F. Azimi, *Spectroscopic Characterization Techniques for Layered Double Hydroxide Polymer Nanocomposites*, Woodhead Publishing, Sawston, Cambridge **2020**.
[2] P. Gatkine, S. Veilleux, Y. Hu, J. Bland-Hawthorn, M. Dagenais, *Opt. Express* **2017**, *25*, 17918.
[3] B. I. Akca, V. D. Nguyen, J. Kalkman, N. Ismail, G. Sengo, F. Sun, A. Driessen, T. G. V. Leeuwen, M. Pollnau, K. Wörhoff, R. M. D. Ridder, *IEEE J. Sel. Top. Quantum Electron.* **2012**, *18*, 1223.
[4] B. K. Ford, M. R. Descour, R. M. Lynch, *Opt. Express* **2001**, *9*, 444.

[5] D. Melati, P. G. Verly, A. Delâge, P. Cheben, J. H. Schmid, S. Janz, D.-X. Xu, *Opt. Express* **2018**, *26*, 28651.
[6] M. K. Smit, *Electron. Lett.* **1988**, *24*, 385.
[7] D. Dai, Z. Wang, J. F. Bauters, M.-C. Tien, M. J. R. Heck, D. J. Blumenthal, J. E. Bowers, *Opt. Express* **2011**, *19*, 14130.
[8] G. Calafiore, A. Koshelev, S. Dhuey, A. Goltsov, P. Sasorov, S. Babin, V. Yankov, S. Cabrini, C. Peroz, *Light: Sci. Appl.* **2014**, *3*, e203.
[9] B. Momeni, E. S. Hosseini, A. Adibi, *Opt. Express* **2009**, *17*, 17060.
[10] Z. Xu, Z. Wang, M. E. Sullivan, D. J. Brady, S. H. Foulger, A. Adibi, *Opt. Express* **2003**, *11*, 2126.
[11] M. Chakrabarti, M. L. Jakobsen, S. G. Hanson, *Opt. Lett.* **2015**, *40*, 3264.
[12] R. K. Gupta, G. D. Bruce, S. J. Powis, K. Dholakia, *Laser Photonics Rev.* **2020**, *14*, 2000120.
[13] N. K. Metzger, R. Spesyvtsev, G. D. Bruce, B. Miller, G. T. Maker, G. Malcolm, M. Mazilu, K. Dholakia, *Nat. Commun.* **2017**, *8*, 15610.
[14] Y. Wan, X. Fan, S. Wang, Z. Zhang, S. Zhao, Z. He, *J. Lightwave Technol.* **2021**, *39*, 2223.
[15] Y. Wan, S. Wang, X. Fan, Z. Zhang, Z. He, *Opt. Lett.* **2020**, *45*, 799.
[16] G. D. Bruce, L. O'Donnell, M. Chen, M. Facchin, K. Dholakia, *Opt. Lett.* **2020**, *45*, 1926.
[17] S. F. Liew, B. Redding, M. A. Choma, H. D. Tagare, H. Cao, *Opt. Lett.* **2016**, *41*, 2029.
[18] N. H. Wan, F. Meng, T. Schröder, R.-J. Shiue, E. H. Chen, D. Englund, *Nat. Commun.* **2015**, *6*, 7762.
[19] B. Redding, M. Alam, M. Seifert, H. Cao, *Optica* **2014**, *1*, 175.
[20] B. Redding, H. Cao, *Opt. Lett.* **2012**, *37*, 3384.
[21] B. Redding, S. F. Liew, R. Sarma, H. Cao, *Nat. Photonics* **2013**, *7*, 746.
[22] W. Hartmann, P. Varytis, H. Gehring, N. Walter, F. Beutel, K. Busch, W. Pernice, *Nano Lett.* **2020**, *20*, 2625.
[23] D. Yi, Y. Zhang, X. Wu, H. K. Tsang, *IEEE J. Quantum Electron.* **2020**, *57*, 0600108.
[24] B. Redding, S. F. Liew, Y. Bromberg, R. Sarma, H. Cao, *Optica* **2016**, *3*, 956.
[25] Y. Shen, N. C. Harris, S. Skirlo, M. Prabhu, T. Baehr-Jones, M. Hochberg, X. Sun, S. Zhao, H. Larochelle, D. Englund, M. Soljačić, *Nat. Photonics* **2017**, *11*, 441.
[26] T. W. Hughes, M. Minkov, Y. Shi, S. Fan, *Optica* **2018**, *5*, 864.
[27] J. K. George, H. Nejadriahi, V. J. Sorger in *Proc. 2017 IEEE Int. Conf. Rebooting Comput. (ICRC)*, IEEE, Piscataway, NJ **2017**.
[28] Q. Chang, Q. Li, Z. Zhang, M. Qiu, T. Ye, Y. Su, *IEEE Photonics Technol. Lett.* **2009**, *21*, 60.
[29] B. Redding, S. M. Popoff, H. Cao, *Opt. Express* **2013**, *21*, 6584.
[30] C. R. Rao, S. K. Mitra in *Proceedings of the Sixth Berkeley Symposium on Mathematical Statistics and Probability, Theory of Statistics*, University of California Press, Berkeley, CA **1972**.
[31] R. A. Rutenbar, *IEEE Circuits Devices Mag.* **1989**, *5*, 19.
[32] E. J. Candes, M. B. Wakin, *IEEE Signal Process. Mag.* **2008**, *25*, 21.
[33] V. Britanak, P. C. Yip, K. R. Rao, *Discrete Cosine and Sine Transforms: General Properties, Fast Algorithms and Integer Approximations*, Elsevier, New York **2010**.